International Journal of Nanomedicine

Dovepress
open access to scientific and medical research

Open Access Full Text Article

ORIGINAL RESEARCH

The Synergistic Effect of High Intensity Focused Ultrasound on In-vitro Remineralization of Tooth Enamel by Calcium Phosphate Ion Clusters

Barsha Shrestha[1], Sheetal Maria Rajan[1], Sultan Aati[1,2], Emielda Yusiharni[3], Omar Kujan[1], Martin Saunders[4], Amr Fawzy[1]

[1]UWA Dental School, The University of Western Australia, Perth, WA, Australia; [2]Dental Health Department, College of Applied Medical Sciences, King Saud University, Riyadh, Saudi Arabia; [3]UWA XRD Facility, Material & Environmental Analysis Platform, The University of Western Australia, Perth, WA, Australia; [4]Centre for Microscopy, Characterisation and Analysis, The University of Western Australia, Perth, WA, Australia

Correspondence: Amr Fawzy, UWA Dental School, The University of Western Australia, 17 Monash Avenue, Nedlands, WA, 6009, Australia, Tel +61894572434, Email amr.fawzy@uwa.edu.au

Background: Remineralization of dental enamel is an important intervention strategy for the treatment of demineralized lesions. Existing approaches have limitations such as failure to adequately reproduce *both* the ideal structural *and* mechanical properties of the native tooth. The ability of ultrasound to control and accelerate the crystallization processes has been widely reported. Therefore, a new approach was explored for in-vitro enamel remineralization involving the synergistic effect of high-intensity focused ultrasound (HIFU) coupled with calcium phosphate ion clusters (CPICs).

Methods: The demineralized enamel was treated with CPICs, with or without subsequent HIFU exposure for different periods (2.5, 5, and 10 min). The specimens were characterized by scanning electron microscopy (SEM), atomic force microscopy (AFM), and Raman spectroscopy. The surface hardness and crystallographic properties of the treated specimens were evaluated using Vickers microhardness testing and X-ray diffraction (XRD), respectively.

Results: SEM revealed distinct, organized, and well-defined prismatic structures, showing clear evidence of remineralization in the combined CPIC/HIFU treatment groups. AFM further revealed a decrease in the surface roughness values with increasing HIFU exposure time up to 5 min, reflecting the obliteration of interprismatic spaces created during demineralization. The characteristic Raman band at 960 cm^{-1} associated with the inorganic phase of enamel dominated well in the HIFU-treated specimens. Importantly, microhardness testing further demonstrated that new mineral growth also recovered the mechanical properties of the enamel in the HIFU-exposed groups. Critical to our aspirations for developing this into a clinical process, these results were achieved in only 5 min.

Conclusion: HIFU exposure can synergise and significantly accelerate in-vitro enamel remineralization process via calcium phosphate ion clusters. Therefore, this synergistic approach has the potential for use in future clinical interventions.

Keywords: enamel remineralization, high intensity focused ultrasound, calcium phosphate ion cluster

Introduction

Despite significant advancements in dentistry, dental demineralized lesions remain one of the most prevalent diseases worldwide.[1] A non-invasive approach is currently employed to address initial demineralized lesions of dental hard tissues, such as enamel, with remineralization of these tissues being an important therapeutic strategy for early prevention and interception of disease.[2] The enamel demineralization process begins with the dissolution of minerals from the enamel surface due to an imbalance between physiological demineralization/remineralization cycles, with bacteria-mediated and bacteria-free chemical attacks (erosion) being the primary cause of this imbalance and a significant contributor to structural defects in the enamel.[3] Consequently, this leads to clinical complications such as cavities, compromised aesthetics, and function, eventually decreasing the longevity of the tooth.

Received: 3 April 2024
Accepted: 20 May 2024
Published: 6 June 2024

Graphical Abstract

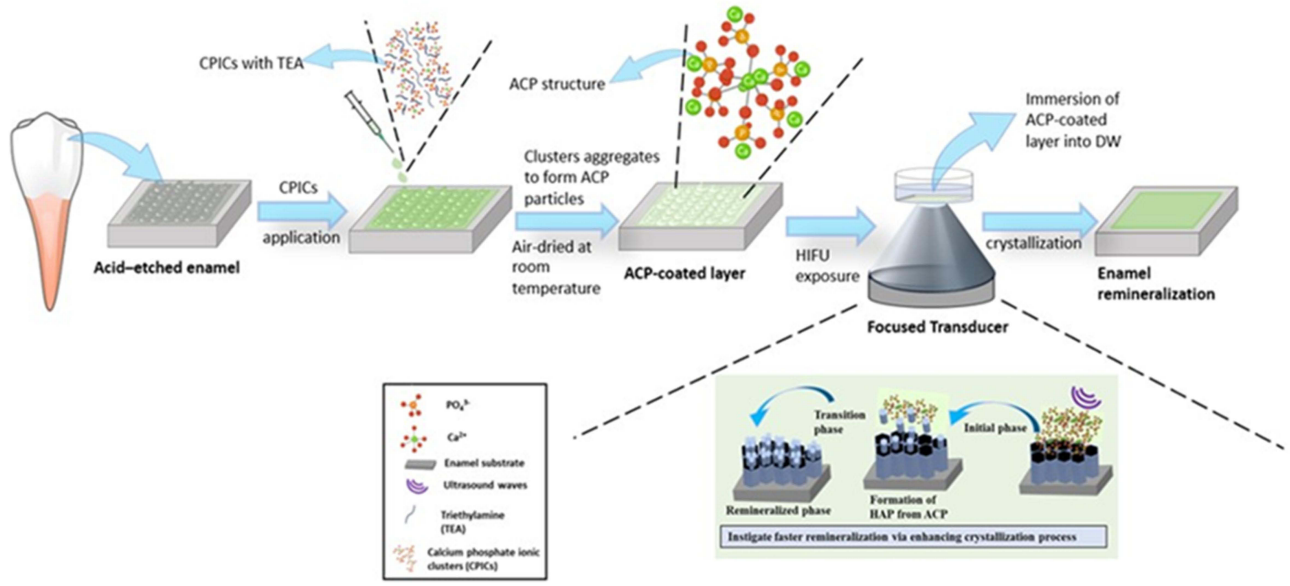

The enamel structure serves as a protective outer shell and the first line of defence to its underlying inner tooth tissues. The defensive properties of enamel are a result of the sophisticated, intricate organization of rod-like hydroxyapatite [HAP; $Ca_5(PO_4)_3(OH)$] crystallites, which are oriented parallel to their *c*-axial direction.[4,5] However, despite being a highly resilient hard tissue in the human body, it does not have the ability to self-repair after being damaged because mature enamel is acellular.[6] Therefore, developing new approach to biomimetic remineralization of enamel capable of restoring the structural integrity and properties of the enamel is of crucial significance.

Fluoride application has been considered the "gold standard" treatment modality for early demineralized enamel lesions. Nevertheless, recent research has revealed the drawbacks and constraints of it: (i) it is incapable of forming ordered mineral crystals within the demineralized enamel surface layer, compromising the mechanical properties of the repaired enamel,[7] and (ii) Fluoride-mediated remineralization is dependent on the bioavailability of Ca^{2+} and PO_4^{3-} ion, which is one of the limiting factor for net remineralizations, and this is exacerbated in hyposalivation conditions.[8,9] Moreover, excessive fluoride exposure could be potentially harmful.[10] Therefore, several attempts have been made to develop alternative treatment interventions aiming to repair initial demineralized enamel lesions. In particular, (i) cell-free strategies such as controlled release of calcium from Ca-EDTA using hydrothermal methods,[11] surfactant-driven HAP self-assembly,[12,13] HAP formation from precursor (amorphous calcium phosphate nanoparticle) assembly;[14,15] (ii) protein/peptide-driven mineralization,[16,17] and (iii) hydrogel-induced remineralization.[18,19] However, all of the aforementioned methods are performed under extreme conditions such as high temperatures and pressures, low pH, or technical complexities and/or high cost (such as those associated with protein-driven mineralization), which could limit their clinical translation.

Synthetic HAP has attracted attention as a substitute biomaterial for tooth enamel due to its chemical similarity to enamel's inorganic components.[20] However, it is not widely used because natural enamel has a complex structure that is difficult to regenerate using synthetic HAP due to variations in the morphologies, phases, and orientations of the crystals in the natural enamel.[21] It is interesting to note that in the natural enamel, HAP crystallites are thought to form from an amorphous calcium phosphate (ACP) precursor, which is in turn made up of Posner's clusters [$Ca_9(PO_4)_6$], an approximately spherical cluster of ions with a domain size of 0.95 nm.[22–24] Hence, inspired by the aforementioned biological process, enamel repair with calcium phosphate ion clusters (CPICs) has been proposed[25] as a mineralization

frontier for in situ remineralization. However, this approach might not be clinically feasible because the crystallization method employed requires approximately 2 days for remineralization of the enamel layer.

Sonochemical methods have been shown to be a promising approach in the synthesis of nanoparticles from solution owing to their ability to enhance the nucleation process, decrease crystallization time, and improve purity.[26,27] Previous studies have investigated the sonochemical synthesis of size-controlled HAP nanoparticles using a sonication bath and homogeniser.[28–30] High-intensity focused ultrasound (HIFU) has recently attracted attention in the field of dentistry owing to its characteristic properties such as potent drug delivery and ability to induce a variety of bioeffects on biological tissues.[31,32] HIFU is a high-amplitude ultrasonic energy where a transducer generates acoustic cavitation, resulting in (i) physical effects (such as shock waves and a high-velocity microjet) and (ii) chemical effects (such as the formation of radical species).[33] These properties have been reported to accelerate crystallization processes in solution.[33,34] Yusof et al was the first to demonstrate the potential of an HIFU system to synthesise nanoparticles with controlled sizes and shapes.[34]

Here, we introduce a new approach for remineralization of demineralized enamel through the synergistic effect of HIFU coupled with calcium phosphate ionic clusters. The first aim was to assess the effect of HIFU exposure on the transformation of amorphous calcium phosphate into HAP particles and to characterize the resulting HAP particles in terms of their chemical composition and crystalline and structural features. The second aim was to investigate the remineralising effect of HIFU exposure coupled with CPIC application on the repair of demineralized enamel specimens. Remineralized enamel specimens are characterized by their morphological and structural features, surface topography, chemical composition, and mechanical properties.

Materials and Methods

Formulation and Characterizations of Nanoparticles

The calcium phosphate ionic clusters (CPICs) and amorphous calcium phosphate (ACP) nanoparticles were prepared as previously described;[25] *detailed information can be found in* supplementary material S1. The prepared nanoparticles were characterized by transmission electron microscopy and Fourier-transform infrared spectroscopy. Furthermore, the biocompatibility of the synthesized nanoparticles was evaluated using an acid phosphate assay (APH) as previously described[35] against human oral fibroblasts with slight modifications before utilising them for remineralization of the demineralized enamel specimens. Detailed data for the methodology can be found in the supplementary material S2

Experimental Set-Up of the HIFU System

A spherically focused, single-element, bowl-shaped piezoelectric ceramic transducer (H-115; Sonic Concepts, Bothell, USA) with a 64 mm diameter, 63.20 mm geometric focus, and resonance frequency of 250 KHz was used for the study. The transducer was driven by an acoustic amplifier (Sonic Concepts, Bothell, USA) using a standard impedance-matching system (50 Ω). The transducer was attached to a transparent coupling cone (C-101, Sonic Concepts, Bothell, USA) to synchronise the ultrasound signals to the specimens and enhance focusing performance. An overview of the HIFU setup is provided in Figure 1a, and the specific configurations for the various experiments are shown in Figure 1b and c (see later sections for further details).

The Effect of HIFU on the Formation of HAP from CPICs

Nanoparticle Synthesis

HAP particles were formed from CPIC and ACP precursors synthesized according to the methods described above. The HIFU transducer with the coupling cone was submerged in a water tank filled with degassed water (Figure 1b). The CPIC suspension was dried in a glass vial to form a layer at the bottom. Distilled water was then added to the vial, which was placed on top of the cone to ensure the correct focal length and exposed for different times (1.25 min, 2.5, 5, 10, 20, 30, and 40 min) at 30 W, as shown in Figure 1b. To serve as a control, HAP was also formed using a previously described protocol[25] involving incubating of ACP nanoparticles at 37°C for 48 h. A second sample was prepared using this method and a 40-min incubation time (the longest HIFU exposure in our experiment).

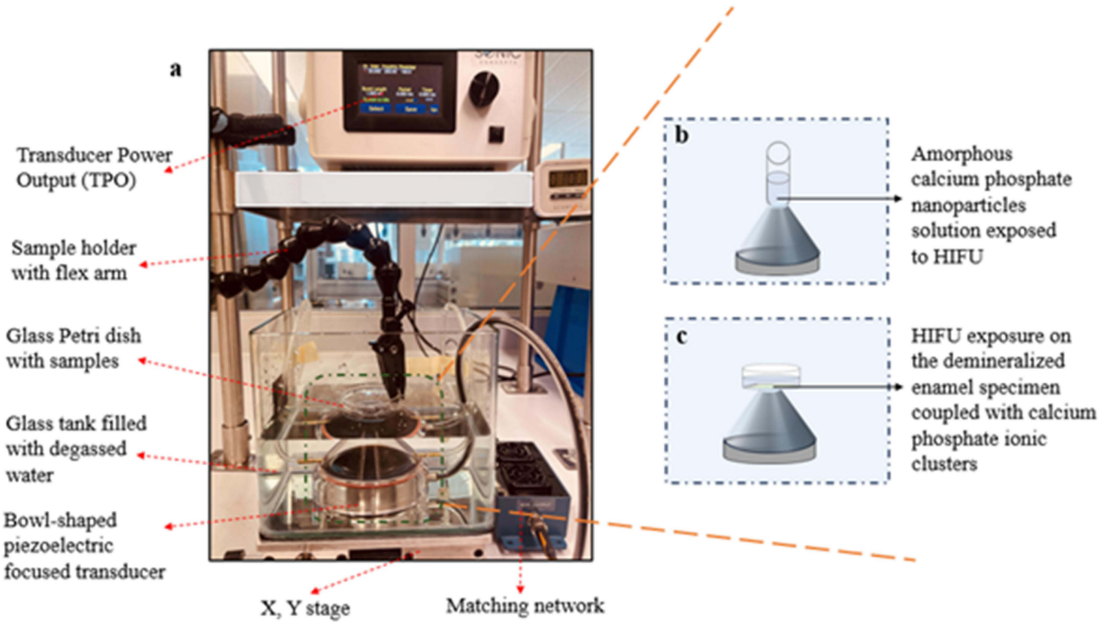

Figure 1 (**a**) Overview of the high intensity focused ultrasound (HIFU) experimental set-up. (**b**) Configuration for assessing the effect of HIFU on the formation of nano-HAP. (**c**) Configuration for investigating the potential of HIFU in synergizing the remineralization process of demineralized enamel specimens treated with calcium phosphate ionic clusters.

Characterization of the Synthesized HAP

The phases of the as-synthesized nanoparticles were confirmed by X-ray diffraction (XRD) using the Bragg-Brentano geometry in an Aeris benchtop X-ray diffractometer (Malvern Panalytical, UK) with monochromatic Co Kα radiation (λ= 1.78 A°) at 40 kV and 15 mA. The data were collected over a 2θ range of 3–80° with increments of 0.0110° and a scanning rate of 0.38 sec/step. The morphology of the nanoparticles was analysed using a transmission TEM (JEOL F200 CF-HR, Tokyo, Japan) equipped with a Gatan OneView camera. Specimens for TEM imaging were prepared by drop-casting suspensions of particles in ethanol onto carbon-coated copper TEM grids.

Enamel Sample Preparation and Demineralization

Sound human premolars (*n = 132*) were selected and stored in 0.1% thymol solution at 4°C. The selected teeth were carious free and were extracted either due to periodontitis or for orthodontic reasons. Ethical approval was obtained from The University of Western Australia Human Research Ethics Committee (Re 2019/RA/4/20/5863). All teeth utilised in the study were obtained from the Teeth Bank at the University of Western Australia, Dental school, where patients had provided consent for the use of their extracted teeth for research purposes. The enamel slabs were obtained from the labial surfaces ($3 \times 3 \times 2$ mm^3) of premolars using an Isomet low-speed diamond saw and then polished with 80-, 1000-, 1500-, 2000-, and 4000-grit silicon carbide discs, followed by ultrasonication in distilled water (DW) to remove residue. The prepared enamel slabs were subjected to 37% phosphoric acid for 30s to create the initial demineralization model,[36] followed by rinsing with distilled water and ultrasonication for 5 min and were stored at 4°C prior use.

HIFU Assisted Remineralization of the Demineralized Enamel

Remineralization of demineralized enamel was performed using CPICs in conjunction with HIFU exposure. Cytotoxicity evaluation of the CPICs was performed against human oral fibroblasts before application to demineralized enamel (see supporting file 1 for more details). Briefly, the CPICs-ethanol solution was dropped onto the demineralized enamel surface and air-dried at room temperature until the formation of an amorphous layer on the enamel surface was observed. Then, the specimens were assigned to different control and experimental groups depending on enamel surface treatment, as follows: (1) demineralized etched enamel with no treatment; (2) CPICs nanoparticle application without HIFU exposure [NP alone]; (3) HIFU exposure for 10 min without CPICs application [HIFU alone]; (4) CPICs application

followed by HIFU exposure for 2.5 min [NP + HIFU (2.5 min)]; (5) CPICs application followed by HIFU exposure for 5 min [NP + HIFU (5 min)]; and (6) CPICs application followed by HIFU exposure for 10 min [NP + HIFU (10 min)]. In Group (2), the treated enamel specimens were immersed in distilled water and incubated at 37°C for 10 min (the maximum duration of HIFU exposure). The exposure times set for enamel remineralization were selected based on the results of the initial time-series experiment investigating the impact of HIFU on HAP nanoparticle formation (see HIFU-accelerated synthesis of crystalline HAP nanomaterials).

The HIFU experimental setup for remineralization of demineralized enamel is shown in Figure 1c. The transducer (250 KHz) was then submerged in a tank filled with degassed water. The specimens treated with CPICs were then transferred to a glass petri dish filled with DW, placed on top of the coupling cone, and exposed for different durations (2.5, 5, and 10 min).

Characterization of Remineralized Enamel Specimens

Scanning Electron Microscopy (SEM)

After treatment, the surface morphologies of the enamel were viewed using a scanning electron microscope (Verios XHR SEM, Thermo Fisher Scientific, US) coupled with energy-dispersive X-ray spectroscopy (EDS, Oxford Instruments X-Max SDD, UK) (n=3/group). The specimens were mounted on aluminium stubs with copper tape and sputter coated with platinum. Secondary electron images were acquired using an Everhart-Thornley detector at an accelerating voltage of 10 kV, and EDS spectra were acquired at 15 KV.

Atomic Force Microscopy (AFM)

The surface topography and roughness of the treated enamel specimens were further investigated by AFM (Cypher VRS, Oxford Instruments, UK). AFM was performed in tapping mode using a platinum-coated beam-shaped cantilever (HQ: XSC11/Al BS; MikroMash; Sofia, Bulgaria) with dimensions of 100 × 50 × 2.7 μm^3 and a radius of < 8 nm. AFM images were obtained with a field view of 10 µm × 10 µm and 256 × 256 pixels per image, resulting in a pixel size of approximately 40 nm (n = 3/per group). The surface roughness was assessed by measuring the average deviation of the surface height relative to its mean to provide the three-dimensional 'average roughness' parameter (S_a) using Gwyddion software (Gwyddion 2.62; Czech Metrology Institute, CZ). The measurements were repeated for five different 10 µm × 10 µm areas to obtain the mean and standard deviation.

Raman Spectroscopy

A Raman microscope (WITec alpha 300RA; Germany) equipped with a laser with an excitation wavelength of 785 nm was used for biochemical analysis of the treated specimens. The instrument was calibrated using a silicon wafer to produce a standard Raman peak at 520 cm^{-1}. The enamel specimens from each group were placed on glass slides and on a sample stage. After focusing on the sample surface at 20 × magnification, optical images were obtained using an air objective. The signal from the sample surface was acquired using a 600-line per mm diffraction grating centred at 973 cm^{-1}, using a spectrometer equipped with an Andor iDUS 401 CCD maintained at −60°C. The spectrum of each enamel specimen was collected with an integration time of 1 s and summing 20 repeat acquisitions from each location. After acquisition, all spectra were analysed using the Project Five software. Each acquisition was repeated at 10 different locations, and the average peak intensity across the 10 measurements was reported. Peak heights were measured after background subtraction.[37]

X-Ray Diffraction (XRD)

The crystal orientations and mineral phases of the treated enamel specimens were evaluated by X-ray diffraction (XRD). XRD patterns of the etched enamel specimens were first recorded over a 2θ range of 10–60° with an increment of 0.0110° in an Aeris benchtop X-ray diffractometer (Malvern Panalytical, UK) with cobalt radiation (λ= 1.78 A°) at 40 kV and 15 mA. Specimens exposed to HIFU were analysed both before and after HIFU exposure to investigate any crystallographic changes induced by HIFU during the remineralization process.

Surface Microhardness

Microhardness of the specimen surfaces was measured using a microhardness tester (Duramin-40; Struers, Australia) equipped with a Vickers indenter. Specimens from each group (n = 10) were tested before and after the treatment. A load of 100 g was applied to the surface for 10 s using a pyramid-shaped diamond indenter. For each specimen, 15 indentations were made, and the results are reported as the average of the indented locations for each treated specimen. The surface microhardness recovery was calculated using the following formula:[38]

$$\mathrm{SMHRR}\,\% = (\mathrm{SMH2} - \mathrm{SMH1})/(\mathrm{SMH0} - \mathrm{SMH1}) \times 100 \quad (1)$$

Where,

SMH0 = surface microhardness of sound enamel (baseline)
SMH1 = surface microhardness of demineralized enamel
SMH2 = surface microhardness of remineralized enamel

Statistical Analysis

A sample size calculation was performed utilizing G*Power software (ver. 3.1.9.7; Heinrich-Hein-Universität Düsseldorf, Düsseldorf, Germany); with an effect size of f = 0.4, α err prob = 0.05, and power = 0.8/0.9, resulted in a total minimum sample size of 132 for the study. All data are presented as the mean ± standard deviation. One-way ANOVA followed by a post-hoc Tukey's test was performed to determine the statistical differences among the groups at the alpha level ($p < 0.05$). All statistical tests were performed using SPSS (Version 23.0, IBM Armonk, NY, US).

Results and Discussion

Formulation and Characterization of Synthesized Nanoparticles

The morphological structures of the synthesized nanoparticles were investigated using TEM (Figure 2a and b). The CPICs nanoparticles appeared as small, round particles with an average diameter of 1.2 nm (Figure 2a). These small particles assembled and aggregated to form larger, amorphous, spherical ACP nanoparticles (Figure 2b), consistent with the findings of Shao et al.[25] Elemental analyses revealed that ACP formed from CPICs nanoparticles consisted of three major elements, O, Ca, and P which were homogeneously distributed, and no impurities were observed (Figure 2c). The diffuse diffraction pattern (Figure 2b inset) further confirms the amorphous phase.

The FTIR spectra of the CPIC and ACP nanoparticles are shown in Figure 2d. The characteristic peaks at 1022 cm^{-1} and 2948 cm^{-1} were assigned to C-O stretching and C-H stretching, respectively, confirming the formation of CPIC nanoparticles.[23,39] Furthermore, the C-N stretching at 1203 cm^{-1} suggested an interaction between the CPIC nanoparticles and TEA.[23] The prominent peaks at ~567 cm^{-1} and ~1055 cm^{-1} were assigned to the asymmetric O-P-O bending vibration and P-O stretching, respectively,[40] indicating a transition from CPICs to ACP nanoparticles. Moreover, the absence of C-N and C-O bands in the ACP nanoparticle spectrum suggests the removal of TEA and ethanol.

It is important for the nanoparticles to undergo cytotoxicity evaluation before their application to biological specimens to minimise the risk of potential adverse effects. Therefore, a cytotoxicity investigation using human oral fibroblasts was performed at three different time points. The proliferation behaviour of human oral fibroblast cells in the experimental group at 1, 3, and 7 days was similar to that of the control/untreated group (Figure 2e). No statistically significant difference in optical density (OD) difference was observed between the untreated and experimental group ($p > 0.05$), indicating the biocompatibility of the nanoparticles with human oral fibroblasts.

HIFU-Accelerated Synthesis of Crystalline HAP Nanomaterials

ACP was first synthesized from CPICs as previously described.[23] TEM images of ACP exposed to HIFU for various times are shown in Figure 3a–g. For comparison, control specimens in which the crystallization method described in [25] was applied to ACP are shown in Figure 3h and i, for an incubation time of 48 h (the time

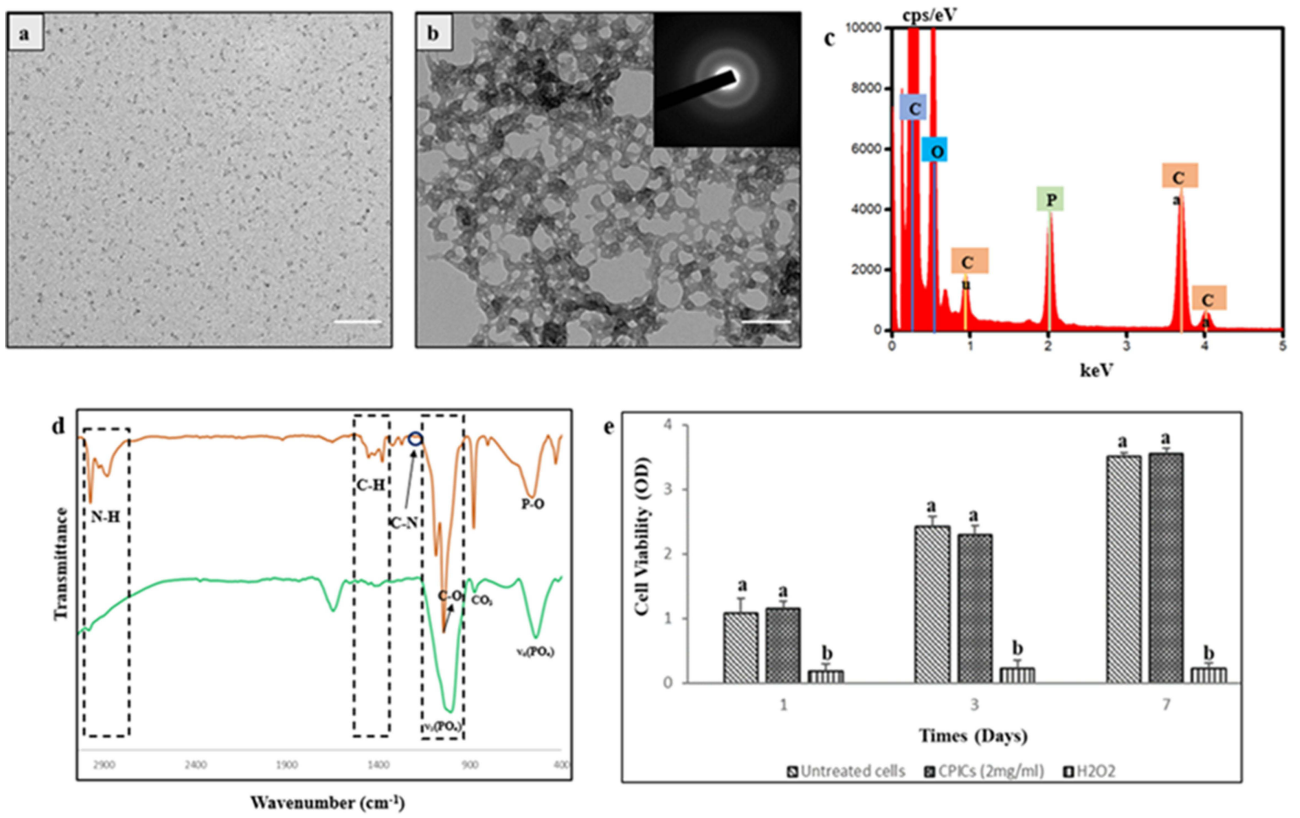

Figure 2 TEM images showing the morphology of the synthesized (**a**) CPICs nanoparticles, and (**b**) ACP resulting from the fusion of CPICs combined with volatilization of TEA and ethanol. Scale bars are 200 nm. Inset in (**b**): Selected area electron diffraction (SAED) of ACP confirming the presence of an amorphous phase. (**c**) TEM-EDS elemental analysis of ACP nanoparticles confirming the presence of Calcium, Phosphorous, and Oxygen. (**d**) The acquired FTIR spectra of synthesized CPICs (Orange spectrum) and ACP nanoparticles (green spectrum). (**e**) Results of acid phosphatase assay testing viability of human oral fibroblasts against formulated gel-like CPICs nanoparticles at different time points. Dissimilar lowercase letters indicate statistical significance difference at $p < 0.05$.

identified in[25] as required for full crystallization) and 40 min (the maximum time of HIFU exposure in our experiments), respectively.

Following 2.5 min of HIFU exposure, the amorphous pre-cursor material began to transform into needle-shaped particles (Figure 3b). After 5 min and 10 min of HIFU exposure, the majority of amorphous nanoparticles were transformed. Longer exposure caused fragmentation of the needle-shaped particles, leading to the formation of needles mixed with plate-like particles (Figure 3g). The result after 10 min of HIFU exposure appeared similar to that obtained after 48 h by the conventional method (Figure 3h), whereas no change was observed in the ACP pre-cursor material after 40 min of incubation (Figure 3i).

The XRD patterns of the HIFU-exposed specimens are shown in Figure 3j. The major diffraction peaks observed were identified as the (002), (211), (300), (310), (222), (213), and (004) planes of HAP by comparison with the standard hexagonal HAP reference (COD – 96-901-0051), confirming the transformation of ACP into crystalline HAP. No trace of secondary crystalline phases of calcium phosphate was detected, except for the 40 min group, where one weak peak identified as brushite (another calcium phosphate phase) was observed. The XRD patterns of the control specimens are shown in Figure 3k. These results confirm that the 40-min control sample did not crystallise, while the 48-h control data were consistent with the outcome of the much shorter HIFU experiments.

To the best of our knowledge, no previous study has investigated the potential effect of HIFU in facilitating the transition of ACP to pure HAP. Our data demonstrate the ability of HIFU to induce rapid crystallization, achieving what conventional approaches produce in 48 h in just a few minutes. Ultrasound is known to induce rapid crystallization in solvents.[26] Acoustic cavitation has been reported to promote micro-scale mixing to accelerate the diffusion of solutes which results in faster nucleation and crystal growth.[41] In our case, acoustic cavitation at the boundary between the ACP

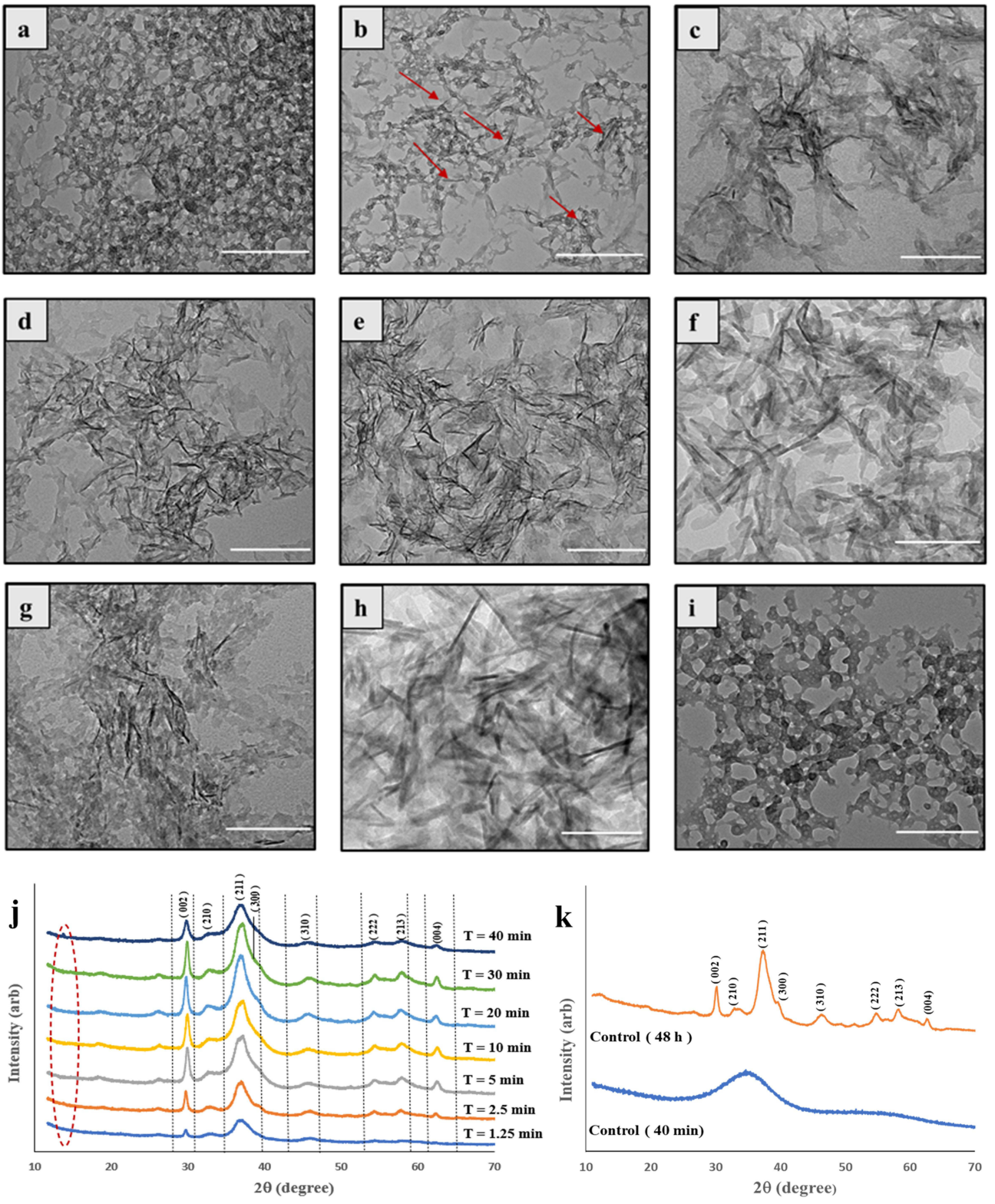

Figure 3 TEM images and XRD patterns of nano-HAP synthesized at different HIFU exposure times. (**a–i**) TEM images of nano-HAP at 1.25 min, 2.5 min, 5 min, 10 min, 20 min, 30 min, 40 min, the controls 48 h and 40 min, respectively. The red arrows in the TEM images indicate formation of needle shape like particles transform from the ACP. (**j**), (**k**) XRD patterns of the experimental groups and the controls respectively. Scale bars represent 200 nm.

and surrounding water is expected to create shock waves and microjets that accelerate the crystallization process, potentially inducing localised heating.[26,27] In addition, HIFU induces the formation of free radicals in water required to convert ACP to HAP.[26,28,41]

HIFU-Enhanced Remineralization of Demineralized Enamel

Inspired by HIFU's ability of HIFU to accelerate the formation of crystalline HAP from ACP, we investigated whether HIFU has a similar synergistic effect on remineralization of demineralized enamel in conjunction with CPICs. In this approach, a demineralized enamel model was created by etching sound polished enamel specimens with 37% phosphoric acid for 30 sec.[36] CPICs were applied to the surface of the demineralized enamel and air-dried to form a layer of ACP. CPIC-treated specimens were exposed to HIFU for 2.5, 5, and 10 min, and were selected based on the outcomes reported in the previous section. The impact of HIFU exposure was investigated using a range of imaging and analytical methods (see the Methods section for details).

Surface Morphology

Secondary electron SEM images of a demineralized enamel substrate showed that the surface was highly porous within the rod cores, with additional loss of material from the interrod region and significant interprismatic gaps (Figure 4a and g). Application of the ACP layer (NP alone group) created a smoother surface, with the amorphous material filling in gaps both within and between the rod cores (Figure 4b–h). Following HIFU treatment coupled with nanoparticle experimental groups, the enamel surface showed decreased microporosity compared to the demineralized sample, and more distinct and well-organised prismatic features than either the demineralized or ACP-coated specimens with increased HIFU exposure time. This indicates that some level of remineralization has taken place (Figure 4d-f and j–l) and that HIFU has not simply removed the CPIC layer to reveal the original demineralized surface.

At higher SEM magnifications, both [NP + HIFU (5 min)] and [NP + HIFU (10 min)] specimens showed significant formation of well-organised crystallites within the central rod and interrod regions (Figure 3k and l). This further indicates that remineralization by [NP + HIFU (5 min)] and [NP + HIFU (10 min)] was more pronounced when compared to all other control and experimental groups. Similar results were obtained in the repair process using CPIC nanoparticles by Shao et al[25] except that their use of a low-temperature incubation step to convert ACP to HAP required 48 h. Exposure to HIFU in the absence of the CPIC layer resulted in less-defined enamel prismatic structures with indistinct crystalline structures (Figure 3c and i), supporting that HIFU exhibits a positive effect on enamel remineralization only if preceded by CPICs application. Furthermore, cross-sectional images of the NP + HIFU (5 min) sample showed that the top few microns of the HIFU-treated sample were denser and contained less porosity and continuous HAP crystallites with a fairly smooth topography (see supplementary material S3). EDS analysis of the NP + HIFU (5 min) sample confirmed that the remineralized layer was composed predominantly of Ca, O, and P, with an approximate Ca:P ratio of 1.8 compared to the 1.7 expected from pure HAP (see Supplementary Material S4). This slight deviation from the ideal value may indicate that some CPIC/ACP remains unconverted by or could simply result from inaccuracies in quantification arising from the rough surface.

While the SEM images provided visual confirmation of the changes in the surface morphology, no quantitative evaluation of the changes in the surface topography could be extracted from the SEM data. Therefore, AFM was used to further investigate the surface topography of the experimental groups. The 2D and 3D AFM images show consistent behaviour with the SEM data, which revealed that the spaces between prismatic structures were filled with new material when demineralized enamel was treated with HIFU coupled with nanoparticles (Figure 5). The demineralized surface showed a globular structure with multiple gaps between the core prism along with greater height variations (Figure 5a), while the experimental groups [NP + HIFU (5 min)] and [NP + HIFU (10 min)] exhibited more of the characteristic prismatic and interprismatic structures of the enamel with less height variations (Figure 5b and c).

These morphological and topographical changes of the repaired enamel surfaces are reflected in the arithmetic average roughness (S_a) values, with the S_a values of the HIFU-treated specimens being significantly decreased compared to the demineralized group (Figure 5g). This reflects the formation of new minerals on the defective enamel surface.[42] Taken together, the SEM and AFM results confirming that remineralization occurred within the defective demineralized

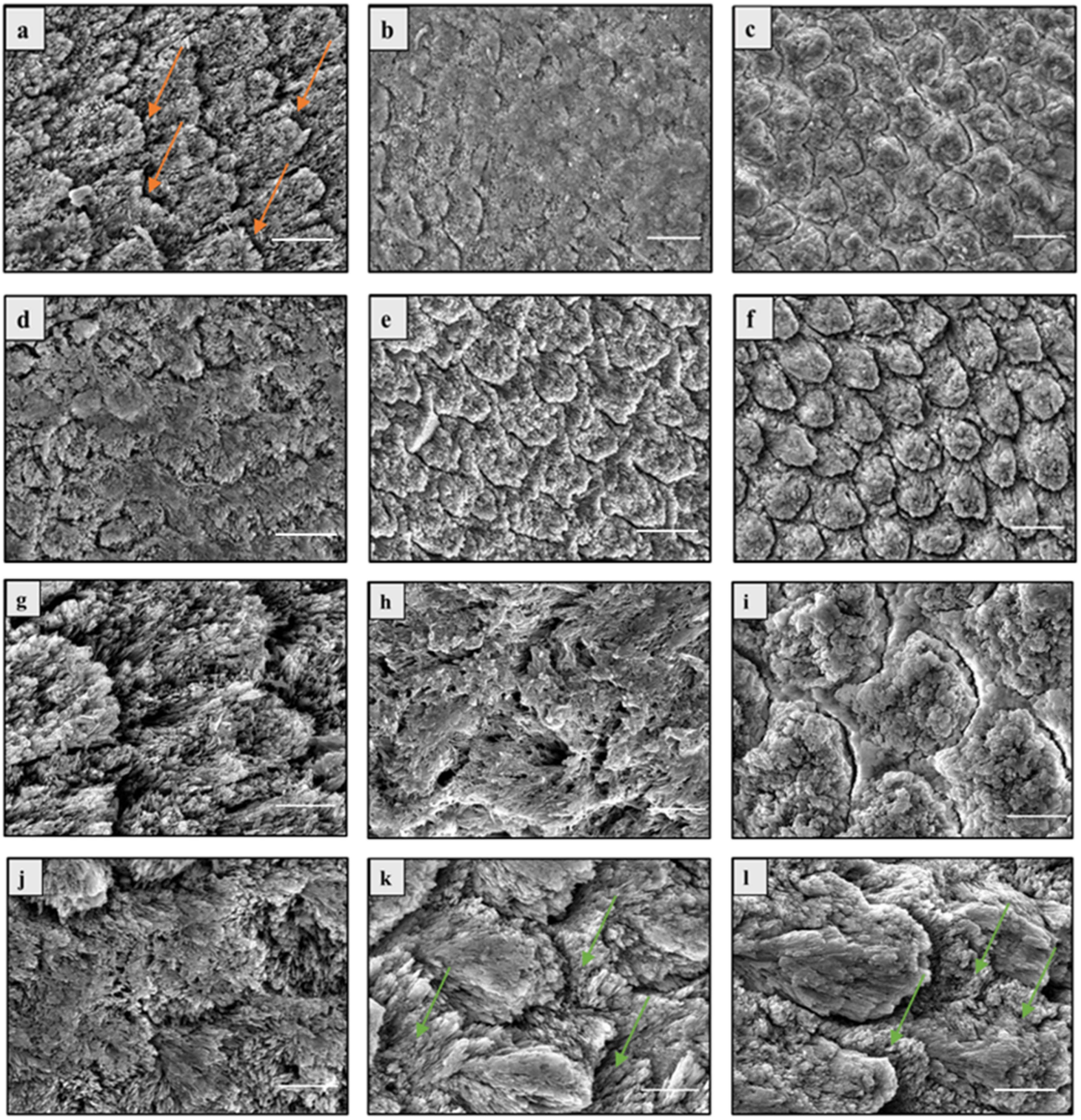

Figure 4 Secondary Electron SEM images of (**a**) demineralized enamel without treatment, (**b** and **c**) treated with [NP alone] and [HIFU alone], respectively; (**d-f**) treated in combination with CPICs and HIFU, exposed for 2.5 min (**d**), 5 min (**e**), and 10 min (**f**), respectively. (**g-l**) corresponding higher magnification images of (**a-f**) SEM images. Scale bars represents 10 µm for (**a-f**) and 3 µm for (**g-l**). Orange arrow depicts loss of HAP crystallites in interrod region; Green arrows in the experimental groups [NP + HIFU (5 min, 10 min)] represents the formation of crystallites within the gap created due to dissolution of mineral ions.

enamel surface utilising external $Ca^{2+}$and PO_4^{3-} ions from CPICs to form new HAP, with the speed of the remineralization process being significantly enhanced by HIFU.

Surface Mineralogy

The Raman spectra of the demineralized enamel and the specimens repaired by HIFU exposure in combination with CPICs are shown in Figure 6a. The Raman intensities of the characteristic peaks of the phosphate groups at approximately 960, 587, and 430 cm^{-1} were assigned to asymmetric bending vibration, asymmetric bending vibration, and

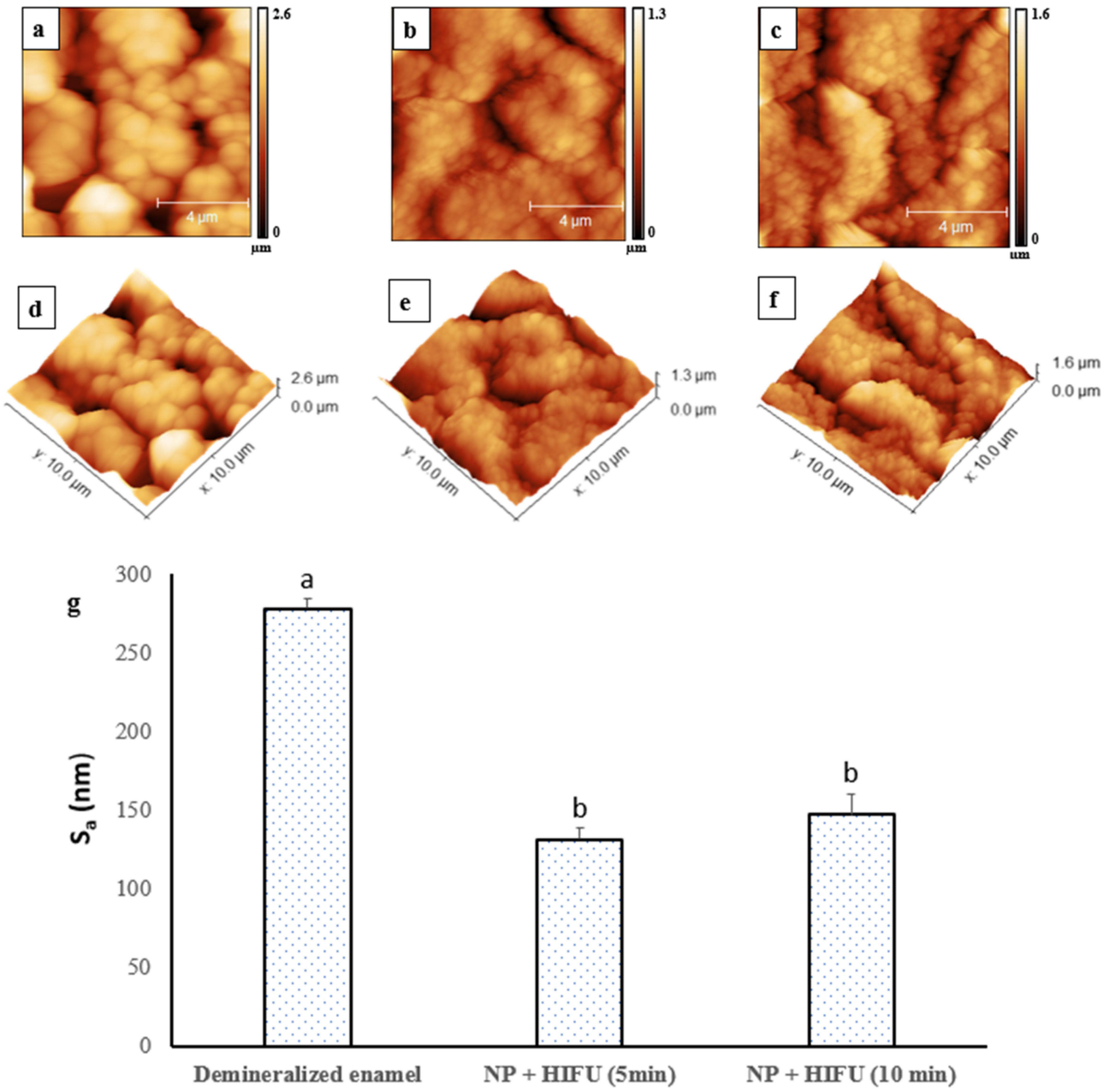

Figure 5 2D and 3D representations of AFM images showing topographical and structural variations between demineralized and HIFU-treated specimens. (**a**) demineralized enamel with no treatment, (**b**) [NP + HIFU (5 min)], and (**c**) [NP + HIFU (10 min)]; (**d,e,f**) corresponding 3D representations; (**g**) average mean roughness value (S_a) of the control and experimental groups. Different letters indicate statistically significant differences ($p < 0.05$). The colour code indicates the scale bar for the height of the image.

symmetric bending vibration, respectively.[43,44] All the experimental groups, [NP + HIFU (2.5, 5, and 10 min)], showed higher phosphate peak intensities than the demineralized sample, indicating an increase in the HAP density in the near-surface region sampled by the Raman spectrometer. The relative intensity of the P-O symmetric stretching mode (ν_1) of PO_4^{3-} at 960 cm^{-1} was highest for the [NP + HIFU (5 min)], followed by [NP + HIFU (10 min)], [NP + HIFU (2.5 min)], and the control. This pattern indicates that more remineralization occurred in the [NP + HIFU (5 min)] and [NP + HIFU (10 min)] specimens because the ν_1 band at 960 cm^{-1} (symmetrical stretching of the tetrahedron of oxygen atoms surrounding the phosphorus atom) is the strongest signal in the Raman spectrum of enamel and is an indicator of the mineral content.[45]

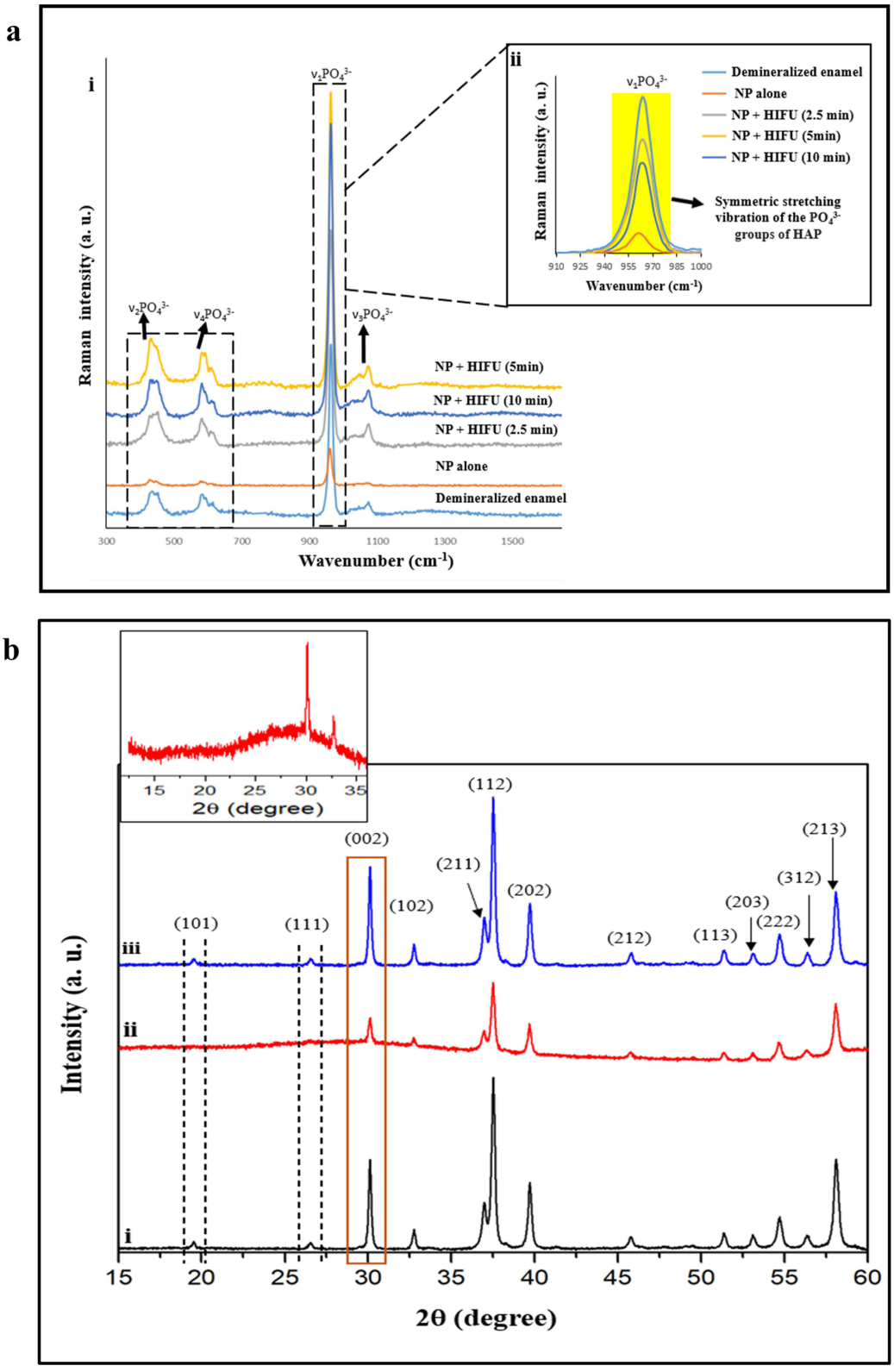

Figure 6 (a) Raman spectroscopy of the demineralized and HIFU-exposed specimens showed an increase in the intensity of characteristic phosphate (v_1 PO_4^{3-}, v_2 PO_4^{3-}, v_4 PO_4^{3-}) in the HIFU specimens; (ii) the Raman intensity at 960 cm^{-1}. (**b**) XRD spectra of (i) demineralized enamel (control); (ii) demineralized enamel specimen treated with CPICs without HIFU exposure; and (iii) [NP + HIFU (5 min)] experimental group; depicting the transformation of amorphous phase into crystalline HAP on the repaired enamel surface. Inset: showing the board peak from 15–35 2θ (degree) of confirming presence of amorphous nanoparticles on the demineralized enamel surface.

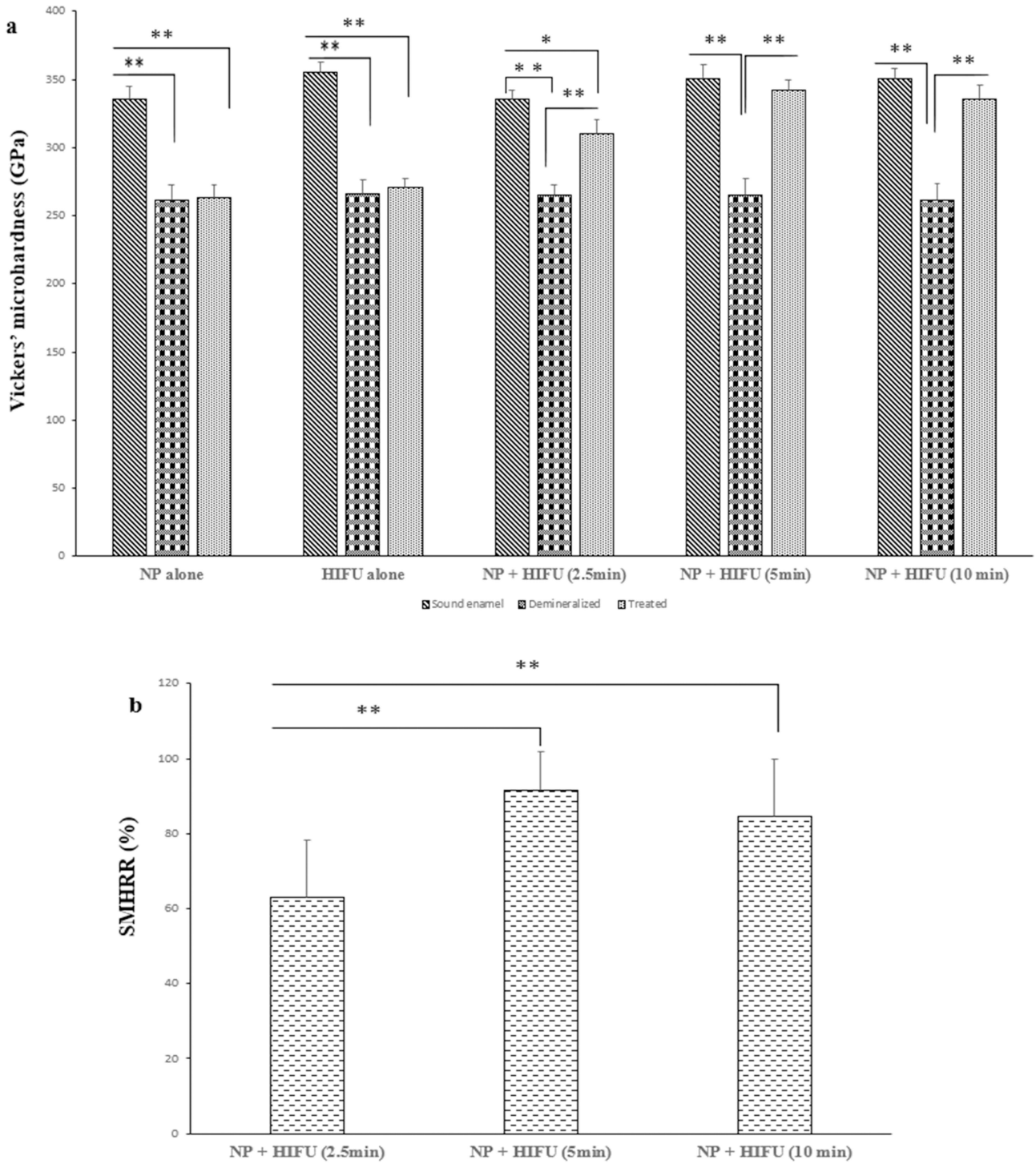

Figure 7 (**a**) The mean ± standard deviation of Vickers microhardness values for the different treated groups (**b**) the percentage of surface microhardness recovery ratio of the three experimental group. The [NP + HIFU (5min)] sample exhibited the highest recovery rate among all the experimental groups. Asterisk symbol indicates statistically significant difference ie, **p < 0.01 and *p < 0.05.

XRD analysis supported this remineralization interpretation (Figure 6b), with the addition of the ACP layer resulting in a broad amorphous peak at 30.15° (line ii), and the application of HIFU (line iii) restoring the strong crystallinity demonstrated in the demineralized sample (line i), with the same set of HAP peaks observed for the HAP nanoparticles (Figure 3). The similarity in the spectra of the demineralized and remineralized specimens confirms that the newly

formed crystalline material has a crystallographic orientation similar to that of the underlying enamel. Overall, both the Raman and XRD data were consistent with the SEM and AFM findings.

Surface Microhardness and Recovery

A key goal of enamel remineralization is to restore *both* the prismatic microstructure *and* mechanical integrity of the enamel. While existing approaches, such as fluoride treatments, have been shown to remineralize the surface, creating new materials that restore the mechanical properties of enamel has proven more elusive.[7,46] Surface microhardness testing of our HIFU-treated enamel specimens confirmed a significant improvement in the mechanical properties of the enamel post-treatment. This means that the mineral content in the demineralized enamel after HIFU treatment coupled with CPICs was restored, as the surface hardness analysis directly reflects the degree of enamel mineralization.[47]

As shown in Figure 7, the microhardness of the HIFU-treated specimens [NP + HIFU (5 min)] and [NP + HIFU (10 min)] increased significantly, with values of 342.10 ± 7.075 and 335.68 ± 9.66, respectively), and their respective mean recovery percentages were 92% and 84.5% (Figure 6b). This is in comparison to their demineralized counterpart specimens which exhibited values of 265.46 ± 11.33 and 261.28 ± 12.10 (Figure 6a, $p < 0.05$). No significant difference was observed between the demineralized specimens and those treated with NP or HIFU alone groups ($p > 0.05$) (Figure 7a). Interestingly, no statistically significant difference was observed between the [NP + HIFU (5 min)] specimens and the sound enamel (Figure 7a). This indicates that the regenerated HAP crystallites may have been closely aligned with those of sound enamel,[38] which is consistent with previous study.[25]

Conclusions

In this study, we present a new approach for the remineralization of demineralized enamel through the synergistic action of high-intensity focused ultrasound (HIFU) coupled with calcium phosphate ion clusters (CPICs). In addition to restoring the microstructure of the enamel, microhardness testing confirmed that our synergistic HIFU/CPIC approach also restored the mechanical properties of the enamel to its original state, which is one of the key goals of enamel remineralization. Although several alternative approaches to the restoration of demineralized enamel have been developed, the time required for remineralization to occur often inhibits their translation to clinical treatment. We showed that HIFU exposure can synergise and significantly accelerate the enamel remineralization process via calcium phosphate ion clusters. Therefore, this synergistic approach has the potential for use in future clinical interventions.

Data Sharing Statement

The data are available from the authors upon reasonable request.

Ethics Approval

The Ethical approval was granted by The University of Western Australia Human Research Ethics Committee (Re 2019/RA/4/20/5863).

Acknowledgment

The authors acknowledge the University of Western Australia's support through a 'Scholarship for International Research Fees and International Living Allowance Scholarship (Ad Hoc Postgraduate Scholarships); and the facilities, and the scientific and technical assistance of Microscopy Australia at the Centre for Microscopy, Characterisation & Analysis, The University of Western Australia, a facility funded by the University, State and Commonwealth Governments.

Funding

This study was supported by Australian National Health and Medical Research Council grant (NMHRC, 1188401) and an Australian Dental Research Foundation grant (ADRF, 0080045000900).

Disclosure

Dr Barsha Shrestha reports grants from the National Health and Medical Research Council grant and grants from the Australian Dental Research Foundation grant, during the conduct of the study. Mrs Sheetal Maria Rajan reports grants from the National Health and Medical Research Council and grants from the Australian Dental Research Foundation, during the conduct of the study. Dr Sultan Aati reports grants from the National Health and Medical Research Council and grants from the Australian Dental Research Foundation, during the conduct of the study. Dr Emielda Yusiharni reports grants from the National Health and Medical Research Council grant (NMHRC, 1188401) and grants from the Australian Dental Research Foundation grant (ADRF; 0080045000900), during the conduct of the study. Dr Martin Saunders reports grants from the National Health and Medical Research Council and grants from the Australian Dental Research Foundation, during the conduct of the study. Dr. Amr Fawzy (lead chief investigator) reports grants from the National Health and Medical Research Council grant (NMHRC, 1188401) and grants from the Australian Dental Research Foundation grant (ADRF; 0080045000900), during the conduct of the study. The authors declare no other competing interests in this work.

References

1. World Health Organization. Global oral health status report: towards universal health coverage for oral health by 2030.
2. Torres PJ, Phan HT, Bojorquez AK, et al. Minimally invasive techniques used for caries management in dentistry. A review. *J Clin Pediatr Dent*. 2021;45(4):224–232. doi:10.17796/1053-4625-45.4.2
3. Abou Neel EA, Aljabo A, Strange A, et al. Demineralization–remineralization dynamics in teeth and bone. *Int j Nanomed*. 2016; Volume 11:4743–4763. doi:10.2147/IJN.S107624
4. Beniash E, Stifler CA, Sun C-Y, et al. The hidden structure of human enamel. *Nat Commun*. 2019;10(1):4383. doi:10.1038/s41467-019-12185-7
5. Palmer LC, Newcomb CJ, Kaltz SR, et al. Biomimetic systems for hydroxyapatite mineralization inspired by bone and enamel. *Chem Rev*. 2008;108(11):4754–4783. doi:10.1021/cr8004422
6. Moradian-Oldak J. Protein-mediated enamel mineralization. *Front Biosci*. 2012;17(7):1996. doi:10.2741/4034
7. Fan Y, Sun Z, Moradian-Oldak J. Controlled remineralization of enamel in the presence of amelogenin and fluoride. *Biomaterials*. 2009;30 (4):478–483. doi:10.1016/j.biomaterials.2008.10.019
8. Reynolds E, Cai F, Cochrane N, et al. Fluoride and casein phosphopeptide-amorphous calcium phosphate. *J Dental Res*. 2008;87(4):344–348. doi:10.1177/154405910808700420
9. Vogel GL, Schumacher GE, Chow LC, et al. Ca pre-rinse greatly increases plaque and plaque fluid F. *J Dental Res*. 2008;87(5):466–469. doi:10.1177/154405910808700513
10. Li L. The biochemistry and physiology of metallic fluoride: action, mechanism, and implications. *Crit Rev Oral Biol Med*. 2003;14(2):100–114. doi:10.1177/154411130301400204
11. Chen H, Tang Z, Liu J, et al. Acellular synthesis of a human enamel-like microstructure. *Adv Mater*. 2006;18(14):1846–1851. doi:10.1002/adma.200502401
12. Chen H, Clarkson BH, Sun K, et al. Self-assembly of synthetic hydroxyapatite nanorods into an enamel prism-like structure. *J Colloid Interface Sci*. 2005;288(1):97–103. doi:10.1016/j.jcis.2005.02.064
13. Fowler CE, Li M, Mann S, et al. Influence of surfactant assembly on the formation of calcium phosphate materials—A model for dental enamel formation. *J Mater Chem*. 2005;15(32):3317–3325. doi:10.1039/b503312h
14. Li L, Mao C, Wang J, et al. Bio-inspired enamel repair via Glu-directed assembly of apatite nanoparticles: an approach to biomaterials with optimal characteristics. *Adv Mater*. 2011;23(40):4695–4701. doi:10.1002/adma.201102773
15. Yamagishi K, Onuma K, Suzuki T, et al. A synthetic enamel for rapid tooth repair. *Nature*. 2005;433(7028):819. doi:10.1038/433819a
16. Yang Y, Lv X, Shi W, et al. 8DSS-promoted remineralization of initial enamel caries in vitro. *J Dental Res*. 2014;93(5):520–524. doi:10.1177/0022034514522815
17. Mukherjee K, Ruan Q, Nutt S, et al. Peptide-based bioinspired approach to regrowing multilayered aprismatic enamel. *Acs Omega*. 2018;3 (3):2546–2557. doi:10.1021/acsomega.7b02004
18. Cao Y, Mei ML, Q-L L, et al. Agarose hydrogel biomimetic mineralization model for the regeneration of enamel prismlike tissue. *ACS Appl Mater Inter*. 2014;6(1):410–420. doi:10.1021/am4044823
19. Ruan Q, Siddiqah N, Li X, et al. Amelogenin–chitosan matrix for human enamel regrowth: effects of viscosity and supersaturation degree. *Connective Tissue Res*. 2014;55(sup1):150–154. doi:10.3109/03008207.2014.923856
20. Dorozhkin SV. Synthetic amorphous calcium phosphates (ACPs): preparation, structure, properties and biomedical applications. *Biomater Sci*. 2021;9(23):7748–7798. doi:10.1039/d1bm01239h
21. Li L, Pan H, Tao J, et al. Repair of enamel by using hydroxyapatite nanoparticles as the building blocks. *J Mater Chem*. 2008;18(34):4079–4084. doi:10.1039/b806090h
22. Posner AS, Betts F. Synthetic amorphous calcium phosphate and its relation to bone mineral structure. *Acc Chem Res*. 1975;8(8):273–281. doi:10.1021/ar50092a003
23. Mancardi G, Tamargo CEH, Di Tommaso D, et al. Detection of Posner's clusters during calcium phosphate nucleation: a molecular dynamics study. *J Mat Chem B*. 2017;5(35):7274–7284. doi:10.1039/C7TB01199G
24. Müller WE, Neufurth M, Ushijima H, et al. Molecular and biochemical approach for understanding the transition of amorphous to crystalline calcium phosphate deposits in human teeth. *Dent Mater*. 2022;38(12):2014–2029. doi:10.1016/j.dental.2022.11.013

25. Shao C, Jin B, Mu Z, et al. Repair of tooth enamel by a biomimetic mineralization frontier ensuring epitaxial growth. *Sci Adv*. 2019;5(8):eaaw9569. doi:10.1126/sciadv.aaw9569
26. Bang JH, Suslick KS. Applications of ultrasound to the synthesis of nanostructured materials. *Adv Mater*. 2010;22(10):1039–1059. doi:10.1002/adma.200904093
27. Liu X, Wu Z, Cavalli R, et al. Sonochemical preparation of inorganic nanoparticles and nanocomposites for drug release–a review. *Ind Eng Chem Res*. 2021;60(28):10011–10032. doi:10.1021/acs.iecr.1c01869
28. Zou Z, Lin K, Chen L, et al. Ultrafast synthesis and characterization of carbonated hydroxyapatite nanopowders via sonochemistry-assisted microwave process. *Ultrason Sonochem*. 2012;19(6):1174–1179. doi:10.1016/j.ultsonch.2012.04.002
29. Poinern GE, Brundavanam RK, Mondinos N, et al. Synthesis and characterisation of nanohydroxyapatite using an ultrasound assisted method. *Ultrason Sonochem*. 2009;16(4):469–474. doi:10.1016/j.ultsonch.2009.01.007
30. Poinern G, Brundavanam R, Le XT, et al. Thermal and ultrasonic influence in the formation of nanometer scale hydroxyapatite bio-ceramic. *Int j Nanomed*. 2011;6:2083. doi:10.2147/IJN.S24790
31. Daood U, Fawzy A. Minimally invasive high-intensity focused ultrasound (HIFU) improves dentine remineralization with hydroxyapatite nanorods. *Dent Mater*. 2020;36(3):456–467. doi:10.1016/j.dental.2020.01.005
32. Fawzy A, Daood U, Matinlinna J. Potential of high-intensity focused ultrasound in resin-dentine bonding. *Dent Mater*. 2019;35(7):979–989. doi:10.1016/j.dental.2019.04.001
33. Sander JR, Zeiger BW, Suslick KS. Sonocrystallization and sonofragmentation. *Ultrason Sonochem*. 2014;21(6):1908–1915. doi:10.1016/j.ultsonch.2014.02.005
34. Yusof NSM, Ashokkumar M. Sonochemical synthesis of gold nanoparticles by using high intensity focused ultrasound. *ChemPhysChem*. 2015;16(4):775–781. doi:10.1002/cphc.201402697
35. Aati S, Shrestha B, Fawzy A. Cytotoxicity and antimicrobial efficiency of ZrO2 nanoparticles reinforced 3D printed resins. *Dent Mater*. 2022;38(8):1432–1442. doi:10.1016/j.dental.2022.06.030
36. Ye Y, Lu R, Ren H, et al. Mimicking amelogenesis to remineralize enamel through co-assembly of PTL fibrils and CMC/ACP. *Mater Des*. 2023;226:111654. doi:10.1016/j.matdes.2023.111654
37. Świetlicka I, Kuc D, Świetlicki M, et al. Near-surface studies of the changes to the structure and mechanical properties of human enamel under the action of fluoride varnish containing CPP–ACP compound. *Biomolecules*. 2020;10(5):765. doi:10.3390/biom10050765
38. Cury J, Simoes G, Del Bel Cury A, et al. Effect of a calcium carbonate-based dentifrice on in situ enamel remineralization. *Caries Res*. 2005;39(3):255–257. doi:10.1159/000084807
39. Wang C-H, Mutalik C, Yougbaré S, et al. Calcium phosphate nanoclusters for the repair of tooth enamel erosion. *Nanomaterials*. 2022;12(12):1997. doi:10.3390/nano12121997
40. Jin B, Liu Z, Shao C, et al. Phase transformation mechanism of amorphous calcium phosphate to hydroxyapatite investigated by liquid-cell transmission electron microscopy. *Cryst Growth Des*. 2021;21(9):5126–5134. doi:10.1021/acs.cgd.1c00503
41. Kim HN, Suslick KS. The effects of ultrasound on crystals: sonocrystallization and sonofragmentation. *Crystals*. 2018;8(7):280. doi:10.3390/cryst8070280
42. Poggio C, Ceci M, Beltrami R, et al. Atomic force microscopy study of enamel remineralization. *Annali di stomatologia*. 2014;5(3):98.
43. Tsuda H, Arends J. Orientational micro-Raman spectroscopy on hydroxyapatite single crystals and human enamel crystallites. *J Dental Res*. 1994;73(11):1703–1710. doi:10.1177/00220345940730110501
44. AC-T K, Choo-Smith L-P, Hewko M, et al. Ex vivo detection and characterization of early dental caries by optical coherence tomography and Raman spectroscopy. *J Biomed Opt*. 2005;10(3):031116–031118. doi:10.1117/1.1915488
45. Mohanty B, Dadlani D, Mahoney D, et al. Characterizing and identifying incipient carious lesions in dental enamel using micro-Raman spectroscopy. *Caries Res*. 2013;47(1):27–33. doi:10.1159/000342432
46. Yang X, Wang L, Qin Y, et al. How amelogenin orchestrates the organization of hierarchical elongated microstructures of apatite. *J Phys Chem A*. 2010;114(6):2293–2300. doi:10.1021/jp910219s
47. Akkus A, Karasik D, Roperto R. Correlation between micro-hardness and mineral content in healthy human enamel. *J Clini Expl den*. 2017;9(4):1.